http://dx.doi.org/10.5012/bkcs.2011.32.11.4121

Proton-Beam Induced Modifications in the Structural and Optical Properties of YSZ

Tae-Hyung Kim, Boo-Hyung Ryu,† and In-Ja Lee*

*Department of Chemistry and †Department of Safety and Environmental Engineering, Dongguk University, Gyeongbuk 780-714, Korea. *E-mail: lij@dongguk.ac.kr*
Received August 25, 2011, Accepted September 21, 2011

Key Words : YSZ, GAXRD, UV-vis, Proton beam

Yttria-stabilized zirconia (YSZ) is a well-known solid ionic conductor used in oxygen sensors and solid oxide fuel cell.[1-4] Its high ion conductivity at high temperatures is rooted in the oxygen vacancies originally present in the crystal. YSZ is also a promising refractory material suitable as a host for actinide transmutation.[5] The ion irradiation effects of fully stabilized YSZ have been extensively investigated[5-19] and the results show that YSZ exhibits exceptional damage resistance to the neutron[6] and heavy ions.[7-19] YSZ does not undergo amorphization under the irradiation of heavy ions as well as electrons and neutrons.[6,9] Its amorphization was observed only under the Cs ion beams so far.[11,12] From the EPR spectroscopic studies,[13,14] Costantini *et al.* showed that the heavy ion irradiation created the same kinds of color centers in YSZ single crystal as the swift electron irradiation. The damage in YSZ induced by heavy ions irradiations also has been studied by optical spectroscopy,[7,13,15,16] TEM,[7,8,11,12,15,17] RBS,[8,10,12] XPS,[15] and XRD.[8,19] However, the damage in YSZ under the ion irradiation has still not been fully understood and especially, little attention has been given to the study of proton-implanted YSZ. In this study, we investigated the proton-induced change in the microstructure and the optical properties of YSZ by XRD and UV-vis spectroscopy.

The sintered pellets are white and 800 μm thick. The SEM image of the pellet shows few pores. This result is in chime with the fact that the density measured by Archimedes' method is greater than 98% of the theoretical density. Upon irradiation with 120 keV proton beams, the front surface of the pellet turns into pale purple while its back side remains unchanged. As the fluence increases, the color gets darker and finally becomes black at the fluence of 1×10^{18} ions/cm^2. Figure 1 shows the absorption spectra of pellets implanted with 120 keV protons at the fluence ranges of $1 \times 10^{15} \sim 5 \times 10^{16}$ ions/cm^2. It clearly shows that the spectra change with the ion irradiation. The pristine YSZ pellet exhibits a broad absorption band at ~270 nm while no bands in the visible region. Upon exposure to the proton beams, a broad band starts growing at 515 nm (λ_{max}). Its optical density increases with the ion fluence without changing its band shape until the ion fluence reaches up to 5×10^{16} ions/cm^2.

From the ESR and UV-vis spectroscopic studies,[13,14] Costantini *et al.* showed that two types of color centers are produced in YSZ when irradiated with swift electrons and heavy ion beams. One is F^+-type center and the other is T-center. The purple F^+-type center, which is assigned to singly ionized oxygen vacancy, has an absorption band at around 500 nm while yellow T-center reveals its absorption band at 375 nm. Therefore, we attributed the absorption band located at 515 nm to F^+-type center. The color and UV-vis spectra of pellets implanted with 120 keV Xe ions behave in a similar manner to those of proton-implanted YSZ. It seems to indicate that both protons and Xe ions produce same kinds of defects in YSZ.

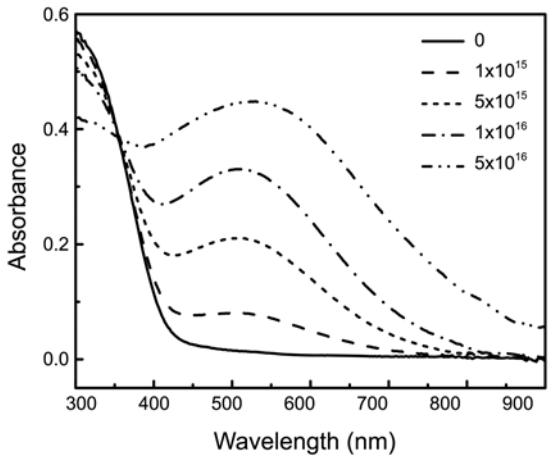

Figure 1. UV-vis spectra of YSZ pellet irradiated with proton beam. The numbers in the figure represent the ion fluence in ions/cm^2.

The growth of the optical density with the formation of F^+-type center can be expressed as follows:

$$A = A_o\{1-\exp(-\sigma Pt)\}$$

where A is absorbance, A_o is the asymptotic value of the absorbance, σ is cross section, P is ion flux and t is irradiation time. At low fluence, the equation is simplified to $A \sim A_o\sigma Pt$. Figure 2 is the plot of the absorbance at 515 nm *vs.* the fluence. It shows that the optical density linearly grows with the ion fluence in the initial stage of the irradiation and then gradually saturated. From the least-square fit of the above equation to the experimental data, A_o and σ are estimated at 0.46 and 1.3×10^{-16} cm^2, respectively. The σ value is in reasonably good agreement with those obtained for YSZ implanted with Ni, Br, I and Au ions.[13]

In order to figure out the relationship between the color

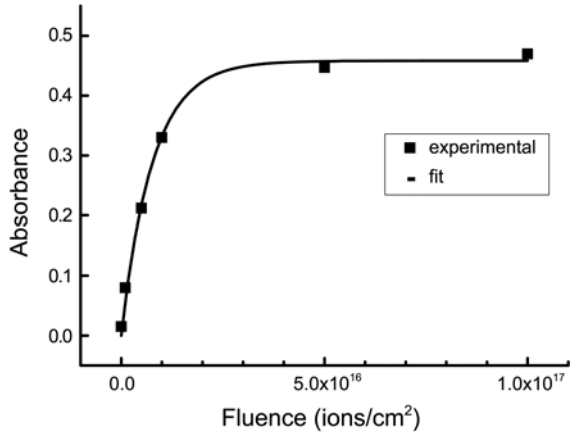

Figure 2. Plot of absorbance *vs*. fluence. The symbols represent experimental data and the solid line is least-square fitted curve using $A=A_o\{1-\exp(-\sigma Pt)\}$.

change and the microstructure of YSZ, XRD patterns of YSZ were measured before and after the proton irradiation and presented in the Figure 3. The patterns obtained prior to the ion implantation, (a), show that the pellet has almost identical XRD pattern with the powder but has narrower peak. The results indicate that both forms of YSZ have cubic fluorite structure but the pellet has larger crystallite size than the powder form due to the sintering process. (b) represents XRD patterns of pellets implanted with 120 keV and 5 MeV protons at the fluence of 5×10^{16} ions/cm^2. Since the color has been changed under the ion irradiation, some sort of surface modification of the crystal structure was expected. However, their XRD patterns are almost identical to those of powder and pristine pellet. No change in the XRD pattern may be explained either by that the concentration of the defects created is too low to be detected by XRD or by that the θ-2θ scan XRD measurement is improper to detect the surface modification of the sample. The ions implanted into the solid materials do not spread evenly but stop at the specified depth of the medium. The SRIM[20] calculation predicts that 120 keV protons range between 300 and 780 nm with the maximum ion density at 610 nm while 5 MeV protons are implanted at about 109 μm. Since the penetration depth of X-ray is ~μm in YSZ,[19] any modification induced by 5 MeV protons cannot significantly contribute to the θ-2θ XRD signal while the defects induced by 120 keV proton beams may contribute to the XRD signal in part.

To examine possible modifications of the surface structure caused by the implantation process, glancing angle x-ray diffraction (GAXRD) was employed and its results were

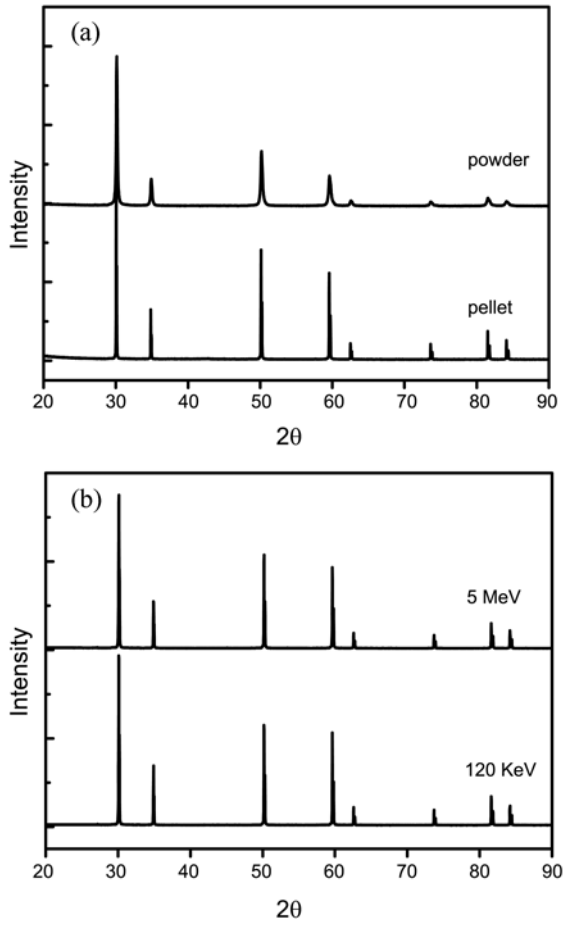

Figure 3. θ-2θ scan XRD data of YSZ pellets; (a) before and (b) after the irradiation. The pellets were irradiated with 120 keV and 5 MeV protons and the fluence was 5×10^{16} ions/cm^2.

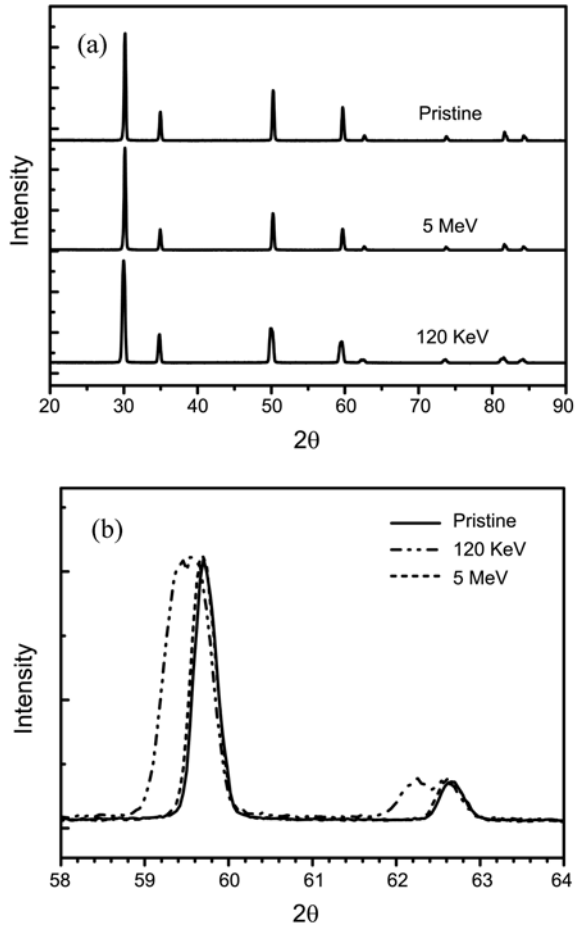

Figure 4. GAXRD pattern of YSZ pellets. (a) $20^o \le 2\theta \le 90^o$ and (b) $58^o \le 2\theta \le 64^o$ region. The pellets were irradiated with 120 keV and 5 MeV protons and the fluence was 5×10^{16} ions/cm^2.

presented in the Figure 4 with the most interesting scales. The incident angle was 1° and its corresponding penetration depth of X-ray is about 140 nm. Overall, the GAXRD patterns of all the intact and proton implanted pellets (5×10^{16} ions/cm^2), (a), are very similar except the wider peak width of the pellet implanted with 120 keV protons. (b), the expanded view of (a) at 57-64° region, indicates that the pattern of the pellet irradiated with 5 MeV protons is identical to that of the pristine. For the implantation with 120 keV protons, however, the peak at 59.7° shifts to 59.5° and is about two times broader than those of the other samples. Meanwhile, a peak at 62.2°, having comparable intensity to the one at 62.6°, is newly observed. Therefore, it seems that the peak located at 59.5° is a convolution of 2 separate peaks, which are located at 59.7° and probably around at 59.3°, respectively. All other peaks behave in a similar manner. We interpret the results to mean that the implanted region of the pellet is also cubic fluorite structure but has the expanded lattice parameter.

The electrolyte material used most for solid oxide fuel cell is YSZ. Since the implanted protons can combine with oxygen site to produce protonic conductive sites, the conductivity is expected to increase under the proton beam. However, the Figure 5, representing the effect of 2.5 MeV proton beams on the conductivity of YSZ as an Arrhenius plot, shows that the conductivity did not vary with the proton beams under the fluence ranges studied. Similar results were obtained for the pellets irradiated with proton beams at higher temperatures. These results seem to indicate that because YSZ is an oxyanion conducting electrolyte, the defects induced by proton beams negligibly contribute to the total conductivity. The inset is the Nyquist plot of the pristine YSZ measured at 400 °C. It shows that the resistance of the bulk and grain boundary are 143 Ω and 25 Ω, respectively.

In summary, YSZ was irradiated with proton beams. Modifications in structural, optical and conductive properties induced by proton beams were investigated by XRD, UV-vis and impedance spectroscopy. Upon irradiation, F^+-like color center (λ_{max} = 515 nm) is linearly produced with the fluence in the initial stage. The calculated implantation depth of 120 keV protons is about to 610 nm. The ion beam did not modify the original crystal structure but results in a longer lattice parameter. The irradiation of proton beams does not improve the conductive property of YSZ.

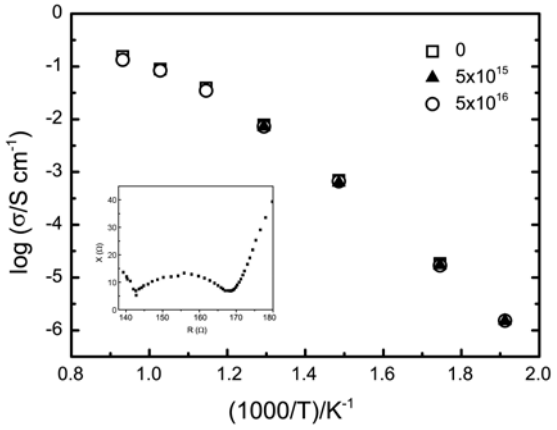

Figure 5. Conductivity of YSZ. The numbers in the figure indicate the proton fluence. The inset is the Nyquist plot of the pristine YSZ measured at 400 °C.

Experimental Section

YSZ powder (Tohso, 8 mol %) was ball-milled for 24 h, dried in oven at 100 °C and then crushed with a mortar. The powder was passed through a mesh (120) to obtain fine powders and calcined at 800 °C for 1 h in the air. Pellets were prepared by uniaxially pressing the powder with 1 ton/cm^2 within a cylindrical mold. Then the pellets were sintered at 1550 °C for 4 h in the air with heating rate of 3 °C/min. Unforced cooling was followed.

The pellets were irradiated with 5 MeV or 120 keV proton beams. The 5 MeV proton-irradiations were carried out using a MC-50 cyclotron in the atmosphere at Korea Institute of Radiological and Medical Sciences. The fluence was adjusted to the range of $1.0 \times 10^{15} \sim 5.0 \times 10^{16}$ ions/cm^2. The 120 keV protons were irradiated under vacuum using an accelerator at Gyeongju branch of Proton Engineering Frontier Project. The fluence was $1.0 \times 10^{15} \sim 5.0 \times 10^{17}$ ions/cm^2.

UV-vis spectra were measured in the spectral range of 300 to 1000 nm using a Cary 5G spectrophotometer (Varian) equipped with an integrating sphere. SRIM 2003[13] was utilized to calculate stopping power and range of ions in matter. The ion energy and the density utilized for the calculation were 120 keV and 6.0 g/cm^3, respectively. The microstructure of sintered pellets was studied by SEM, θ-2θ scan XRD and GAXRD method. In order to obtain directly comparable data, both θ-2θ scan XRD and GAXRD patterns were measured on the same X-ray diffractometer (PANalytical co., X'pert-pro/MPD) using Cu-Kα line, 1.54 Å. The electrochemical properties of the pellet were measured using an AC impedance analyzer (HP, 4192A) by 4-probe method at the frequency range of 5 Hz-13 MHz. For the impedance measurement, both surfaces of the pellet were brushed with Pt paste (TR-7905, Tanaka) and heated to 800 °C for 1 hour.

Acknowledgments. This work was supported by proton Engineering Frontier Project and KRF. XRD was measured at Korea Basic Science Institute.

References

1. Minh, N. Q. *Chemtech.* **1991**, *21*, 120.
2. Minh, N. Q.; Takahashi, T. *Science and Technology of Ceramic Fuel Cells, 92,* Elsevier Science: Amsterdam, 1996.
3. Steele, B. C. H.; Heinzel, A. *Nature* **2001**, *414*, 345.
4. Hibino, T.; Hashimoto, T. *Science* **2000**, *288*, 2031.
5. Gong, W. L.; Lutze, W.; Ewing, R. C. *J. Nucl. Mater.* **2000**, *277*, 239.
6. Savoini, B.; Cáceres, D.; Vergara, I.; González, R.; Muňoz

Santiuste, J. E. *J. Nucl. Mater*. **2000**, *277*, 199.
7. Zhu, S.; Zu, X. T.; Xiang, X.; Wang, Z. G.; Wang, L. M.; Ewing, R. C. *Nucl. Instr. and Meth. B* **2003**, *206*, 1092.
8. Sickafus, K. E.; Matzke, H.; Hartmann, T.; Yasuda, K.; Valdez, J. A.; Chodak, P.; Nastasi, M.; Verall, R. A. *J. Nucl. Mater.* **1999**, *274*, 66.
9. Wang, S. X.; Wang, L. M.; Ewing, R. C. *Phys. Rev. B* **2000**, *63*, 024105.
10. Thomé, L.; Jagielski, J.; Gentils, A.; Garrido, F. *Nucl. Instr. and Meth. B* **2001**, *175*, 453.
11. Wang, L. M.; Wang, S. X.; Zhu, S.; Ewing, R. C. *J. Nucl. Mater.* **2001**, *289*, 122.
12. Vincent, L.; Thomé, L.; Garrido, F.; Kaitasov, O.; Houdelier, F. *J. Appl. Phys.* **2008**, *104*, 114904.
13. Costantini, J.-M.; Beuneu, F.; Gourier, D.; Trautmann, C.; Calas, G.; Toulemonde, M. *Phys.: Condens. Matter* **2004**, *16*, 3957.
14. Costantini, J.-M.; Beuneu , F.. Grynszpan, R. I.; Trautmann, C. *Nucl. Instr. and Meth. B* **2002**, *191*, 616.
15. Xiang, X.; Zu, X. T.; Zhu, S.; Zhang, C. F.; Wang, Z. G.; Wang, L. M.; Ewing, R. C. *Nucl. Instr. and Meth. B* **2006**, *250*, 382.
16. Saito, Y.; Imamura, Y.; Kitahara, A. *Nucl. Instr. and Meth. B* **2003**, *206*, 272-276.
17. Degueldre, C.; Pouchon, M.; Döbeli, M.; Sickafus, K.; Hojou, K.; Ledergerber, G.; Abolhassani-Dadras, S. *J. Nucl. Mater* **2001**, *289*, 115.
18. Sickafus, K. E.; Wetteland, C. J.; Baker, N. P.; Yu, N.; Devanathan, R. D.; Nastasi, M.; Bordes, N. *Mater. Sci. Eng. A* **1998**, *253*, 78.
19. Cheng, J.; Prinz, F. B. *Nucl. Instr. and Meth. B* **2005**, *227*, 577.
20. Ziegler, J. F.; Manoyan, J. M. *Nucl. Instr. and Meth. In Phys. Res. B* **1988**, *35*, 215. Computer program and additional information are available at http://www.srim.org.